Surfaces and Interfaces 83 (2026) 108427

Contents lists available at ScienceDirect

Surfaces and Interfaces

journal homepage: www.sciencedirect.com/journal/surfaces-and-interfaces

Electron spectroscopy investigations of sodium-based battery-relevant reference materials

S. Oswald [a,*], A. Thomas [a], M.V. Gorbunov [a], D. Mikhailova [a,b]

[a] Leibniz Institute for Solid State and Materials Research (IFW) Dresden, Helmholtzstr. 20, 01069 Dresden, Germany
[b] Karlsruhe Institute of Technology (KIT), Institute for Applied Materials (IAM), Hermann-von-Helmholtz-Platz 1, D-76344 Eggenstein-Leopoldshafen, Germany

ARTICLE INFO

Keywords:
XPS
AES
Sodium
Battery
Beam damage
Binding energy shift

ABSTRACT

Electron spectroscopy with X-ray photoelectron (XPS) and Auger electron spectroscopy (AES) is routinely used for characterization of chemical processes occurring in batteries. The coexistence of many possible chemical species at the battery electrodes and energy referencing problems at the mostly insulating surface layers are challenging for the spectroscopic investigations. Here, we present measurement results for reference materials based on the elemental sodium (Na), which is in discussion for the use in stationary energy storage modules. Typical chemical species occurring at the sample surfaces are identified, and beam-induced damage during the experiments is described. Whereas the chemical behavior of metallic Na surfaces is found to be very similar to that for Li and K metal, no substantial intercalation of Na into graphite could be observed.

1. Motivation

In the last decades, rechargeable batteries based on alkaline metal ions Li, Na, K are of high importance for energy storage. Especially Li, which is already being widely used for many industrial applications, dominates the so-called "3C battery market". However, the other alkaline elements Na and K are of interest as well, especially for stationary storage of renewable electric energy. In a plenty of review works (e.g. [1–5]) challenges and further development of metal-ion batteries are discussed.

In this context, the analysis of a complex battery chemistry plays a key role. Since the processes in the battery cells are always related to surface and interface reactions, surface analytical techniques, such as X-ray photoelectron spectroscopy (XPS) and Auger electron spectroscopy (AES) [6–9], are routinely used. Although these techniques have already been applied for a long time, data analysis and identification of various surface chemical species is still challenging [7,10], in particular, due to the high reactivity of the alkaline elements, mostly serving as anodes in half-cells on the laboratory scale. Accordingly, over the last years we studied specially prepared surface states on the alkaline Li and K metals as well as on graphite materials intercalated with these elements [11–15]. The aim was to validate XPS binding energy (BE) reference data for various typical surface species at dedicated surface states. Sample preparation was therefore done under specific conditions: glove box atmosphere and using *in situ* treatment in the analysis chambers. Typically, insulating materials are subjected to investigations, and surface charging occurs. As a consequence, the binding energy (BE) values have to be corrected by energy referencing for reliable identification of the chemical species. We found that the common approach of using the C1s peak of the adventitious carbon on the surfaces at around 285 eV for BE correction [16] is not always straightforward for alkaline materials. In agreement with another report [17], we found typical BE shifts as the result of a "potential barrier" induced by the interface dipole layer between Li or K and non-conducting overlayers [12,17]. Another focus of the previous works comprised investigations of a possible beam damage by the electron beam when using AES for local analysis. This information is important for the complementary use of AES, since XPS is restricted to integral information over relatively large sample areas. Also, a strong interaction with the Ar^+ ion beam used for surface cleaning or element depth profiling was found.

In the current work, we extend the electron spectroscopy studies including instrumental damage effects, from lithium and potassium to sodium and sodium-intercalated graphite materials as an alternative alkali element of interest for use in metal-ion batteries.

From experiments and calculations, the surface chemistry of Li, Na and K after exposition to pure and dry oxygen is expected to be well-defined, with Li_2O on the Li-surface [18], a mixture of Na_2O and Na_2O_2 on the Na-surface [19], and mostly KO_2 on the K-surface [20,21].

* Corresponding author.
E-mail address: s.oswald@ifw-dresden.de (S. Oswald).

https://doi.org/10.1016/j.surfin.2026.108427
Received 8 September 2025; Received in revised form 17 December 2025; Accepted 5 January 2026
Available online 8 January 2026

In our earlier works [11–15], we studied chemical compositions of species formed on the metallic surface of Li and K in an Ar-filled glove box, in which carbonate-based and ether-based electrolytes were in use for battery application. We showed that the metals were always covered by an oxygen-containing layer, which could not be removed by a simple scratching under glove box atmosphere [13]. Thus, mostly a mixture $LiOH/Li_2O/Li_2CO_3$ [13] and K-oxides with a mixed K-valency [15] could be detected, respectively.

Surface chemistry of Na stored under these conditions, with Na_2O, Na_2O_2, NaOH, $NaHCO_3$ and Na_2CO_3 as possible compounds formed on the surface, seems to be more complex [22] and requires a more detailed exploration.

While preparing intercalated graphite reference materials, it is essential to obtain these of highest quality possible. Thereby, as in previous works [14,15], it would be reasonable to use highly-oriented pyrolytic graphite (HOPG) as the intercalation host. With the HOPG it is feasible to prepare smooth bulk-like graphite surfaces *in situ* by delamination with adhesive tapes. Also, it would be preferable to synthesize the graphite intercalation compounds first by a thermal method instead of electrochemical processes, to exclude the influence of electrolyte decomposition products. Although delamination should allow to get rid of the most solid electrolyte interface (SEI) part after the electrochemical routine, homogeneous distribution of guest species within the intercalation host is not always guaranteed.

Chemical intercalation of various guest ions into graphite represents a staging process, meaning a sequential filling of each n^{th} space between the graphene layers. Value n here is assigned to the stage number. Final intercalation compounds (stage 1) for lithium represent LiC_6 while KC_8 for potassium. However, concerning the Na-containing graphite system, it differs significantly from those with lithium and potassium. While chemical synthesis of binary compounds via a reaction with Li or K vapour is relatively simple, it is possible to obtain only NaC_{64} phase under the same conditions [23,24]. From electrochemical reports, it is also well-known that insertion of sodium into graphite does not proceed to the stages with low number n [25]. Thermal synthesis of the lower stage NaC_x compounds would be possible at high pressures, however, they are known to decompose when the pressure is released [26]. Thermodynamic instability of graphite intercalation compounds with high concentration of sodium is also confirmed by theoretical calculations [27]. To summarise, due to the thermodynamic instability at normal conditions, binary Na-graphite compounds with a significant Na fraction were never studied in the conventional XPS setup. Besides, they would be irrelevant for the battery research. Currently, hard carbon materials represent promising alternative anodes for sodium-ion batteries [28].

Nevertheless, it is still possible to apply graphite as an anode for Na-ion batteries, benefitting from the phenomenon of solvent co-intercalation. Jache and Adelhelm [29] described such an intercalation process for glyme-based sodium electrolytes in 2014. Later, Goktas et al. [30] confirmed a good cycling stability despite a huge volume expansion of the graphite-containing electrodes. Since this system is capable of delivering stable electrochemical performance for hundreds of cycles, we decided to consider it in our model experiments. The aim was to explore a chemical composition of the carbon system implying sodium- and glyme-containing species, and its stability under electron beam for AE analysis or Ar^+ beam for sputter cleaning. Solvent molecule decomposition/evaporation cannot be ruled out under beam exposure, leading to interaction between carbon and sodium species.

Another possibility for intercalation of Na into graphite could be in situ deposition of Na at the graphite surfaces, which was already successfully used for doping of fullerene C_{60} [31], also considered as an alternative battery electrode material [32]. This method was tested in our work as well.

Therefore, in the current study we present the XPS results for both, metallic Na samples and products of interaction of Na-species and the graphite material, using various intercalation techniques.

To address the question regarding reproducibility or repeatability of such *in situ*-based experiments, we used a systematically organized experimental strategy for alkali-metal based materials developed in our group during the last decade [11–15]. The presented data are selected from a plenty of measured spectra as representative. Mostly 2-3 samples (metal or HOPG) were prepared in several experiment series and also afterwards investigated in separate XPS/AES measurement series. For each sample, at least three points were measured to ensure the reproducibility.

Although our studies aimed to alleviate understanding surface-relevant (electro)chemical processes in sodium-ion batteries, they rather represent a model experiment because of a quasi-defined and "clean" sample environment (Ar-filled glove-box for preparation and in situ analysis under high-vacuum conditions) comparing to SEI-covered surfaces of electrode materials during/after operation in batteries. Thus, we could avoid any spontaneous surface charging effects upon XPS analysis, while altering effects came only from the residual gas atmosphere. Therefore, we explored spectral results representing simplified and almost unchanged chemical states at the surfaces. However, even our results confirmed a complexity of the sodium surface chemistry making identification of surface species challenging.

This complexity rises tremendously for Na-containing materials in battery cells. Here, on the one hand, a surface charging always occurs due to the thick oxide-containing surface layers, leading to unclear BE definition. On the other hand, mostly mixed chemical species are present, which make their identification challenging. For both aspects our studies deliver the practical solution: a BE referencing considering the potential shift phenomena, and the surfaces and reference spectra for typical surface species, especially the carbonates.

2. Experiments

All sample preparations were done in an Ar-filled glove box (MBRAUN, Germany) with O_2 and H_2O contents less than 0.1 ppm, and with sample transfer to the analysis chambers under the Ar-atmosphere as well, because otherwise only thick-layer oxide products could be observed [22]. Metal Na samples (bulk pieces, Alfa Aesar, Germany, 99% purity) were prepared by cutting the material (stored in oil), cleaning with solvents and scraped with clean scalpels. From the cleaning procedures or electrolyte experiments in the glove box atmosphere, residuals of oxygen containing carbonate- and ether-based substances may still be present on the Na surface.

As a model material for intercalated graphite, highly oriented pyrolytic graphite, HOPG (grade 2, SPI supplies, USA) was used because of its smooth surface and easy delamination for *in situ* preparation of clean surfaces. To test how deep the reaction between graphite and sodium under vacuum occurs, the procedure from our earlier work dedicated to K-intercalation was repeated [15]. This experiment was performed using expanded graphite (obtained from commercial expandable graphite, Sigma Aldrich) instead of HOPG as the intercalation host. After thermal treatment in vacuum, the samples were subjected to powder X-ray diffraction (XRD) in capillaries, at a STOE Stadi P (STOE, Germany) diffractometer, with a CoKα1 radiation and a curved germanium (111 plane) monochromator. The data were collected by a MYTHEN 1 K detector (Dectris). The result of a typical diffraction curve after thermal Na intercalation is compared to that with intercalation of K in the "Supplementary material" (Fig. S1). The only crystalline phase formed under the given intercalation conditions was NaC_{64}, in agreement with the literature data [23,24]. The same conditions afterwards were used for the HOPG intercalation experiment.

Synthesis of a graphite intercalation compound was also done electrochemically following the procedure from [29]. A description of the electrochemical treatment is shown in the supplementary material. In Fig. S2 the galvanostatic discharge curve to a voltage of 0 V vs. metallic Na is shown, resulting in a capacity value of about 56 mAh/g. Afterwards, the intercalated HOPG was taken out from the cell and dried

overnight at 60°C under soft vacuum.

Deposition of sodium in vacuum was done using alkali metal dispensers (SAES getters, Italy) heated by electrical current flow in a separate preparation chamber, which was directly coupled to the XPS system. Base pressure was at 1×10^{-9} mbar. Despite serious outgassing of the getters pressure during deposition was at about 3×10^{-8} mbar. Starting point of the deposition was monitored using a quartz microbalance. Alternating evaporation sequences led to stepwise Na accumulation at the HOPG material for the XPS measurement series.

Despite the glove box preparation, thin oxide layers were always present at the surfaces. They were removed in the analysis chamber. The metals were cleaned by *in situ* scraping or Ar^+ sputtering, while the HOPG by delamination with an adhesive foil. The XPS measurements were mainly performed with a PHI 5600 CI system (Physical Electronics, USA), the AES measurements were done in a JEOL JAMP 9500-F (JEOL, Japan) system, which is additionally equipped with an XPS option. XPS was done with both monochromatic Al-Kα and non-monochromatic Mg-Kα large-area radiation, with a measuring area of approx. 800 μm in diameter determined by the electron analyzer. For AES, an electron beam of 10 keV energy and 10 nA beam current were used. The beam spot size was of around 100 nm in diameter. More detailed information to the specific experimental conditions can be find in the mentioned papers [13–15].

From the spectroscopic point of view, some challenges occurred upon XPS investigations of the Na material. Due to the peak-overlay of the O1s and C1s peaks with Na-KLL Auger lines, the XPS measurements had to be done with both Al- and Mg-Kα X-rays, otherwise the interpretation of carbon and oxygen is erroneous.

The Ar^+ ion-sputtering is routinely used in electron spectroscopy for removing the surface contaminations or for investigation of element distribution in the sample depth. In our study, ion-sputtering was done typically with 3.5 keV (PHI) and 1 keV (JEOL) Ar^+ ions at approximately

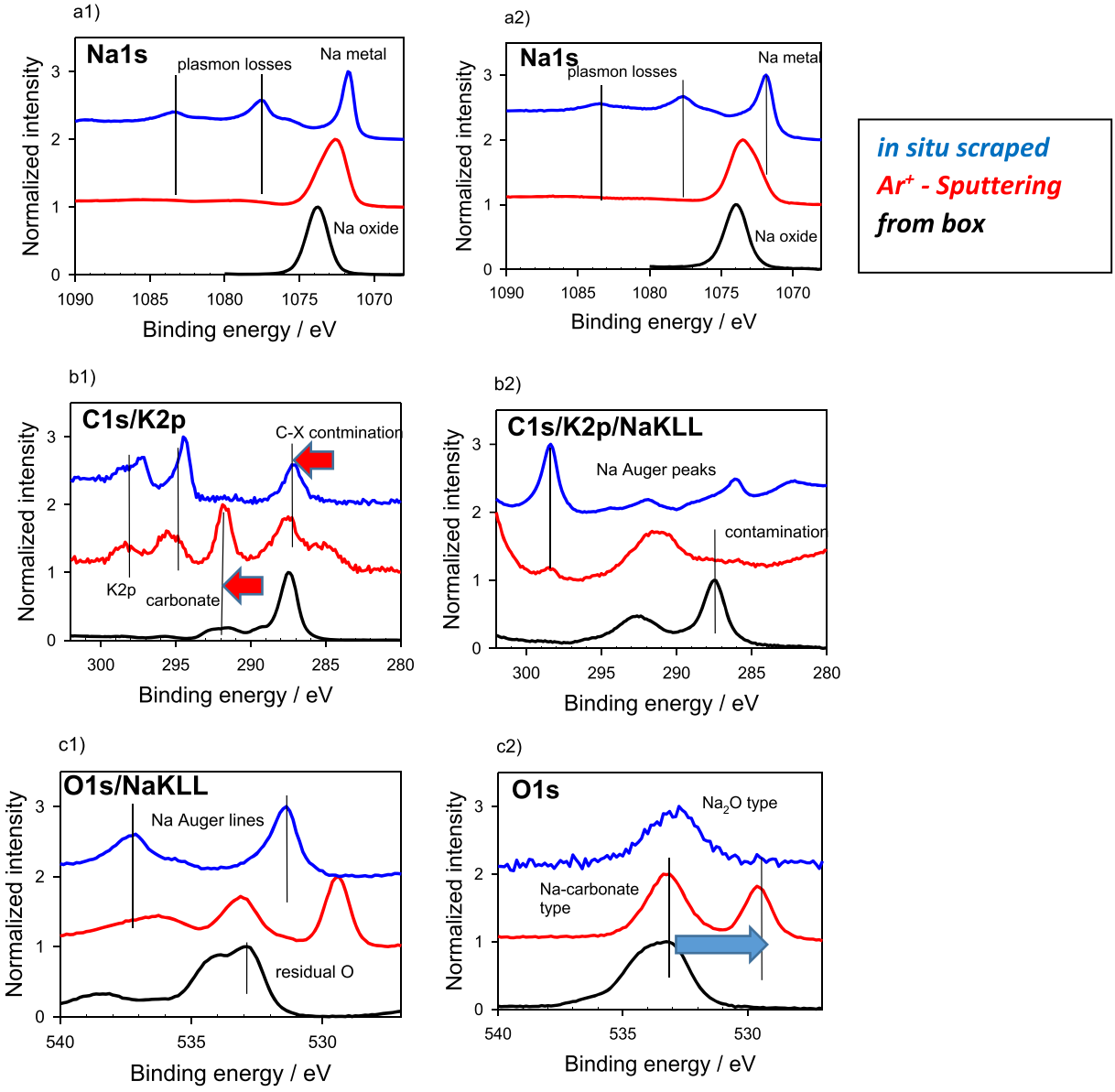

Fig. 1. Normalized XPS spectra of metallic Na samples from the glove box (black), Ar^+ sputter treated (red) and in situ cleaned by scraping (blue) measured with Al-Kα (a1, b1, c1) and Mg-Kα (a2, b2, c2) radiation. The oxide/carbonate-like surface from the box is damaged by sputtering (c2 - blue arrow), the final metallic state is characterized by plasmon loss peaks (a1, a2). Surface contamination peaks (b1) are in high BE position (red arrows). The C1s region is disturbed by NaKLL Auger lines (b2) when measured with Mg-Kα, the O1s region (c1) when measured with Al-Kα.

45° impact angle, resulting in sputtering rates of 3 nm/min and 6 nm/min, respectively.

For the thin reaction layers from this preparation procedures, surface charging was never observed during the measurements, which made separate charge neutralization by charge neutralization or BE shift correction with reference peaks (e.g. C1s at 285 eV) unnecessary. This was regularly checked out by implementation of a low-energy electron beam charge neutralizer or using in addition to monochromatic also non-monochromatic X-rays, which produce a lot of low energy electrons for the measurements. In these cases, we did not observe any significant peak shift or peak broadening. As effect of lateral inhomogeneity or thickness inhomogeneity, a peak broadening would be expected. However, it was not the case here for the overlayer spectra. Obviously, the described interface dipole between alkaline-enriched material and the overlayers is the dominating effect for the observed peak shifts. Using only X-ray excitation during the XPS measurements, no spectral changes were found during the typical measuring times of 10-60 min. Beam-induced spectral and concentration changes, however, could be observed by both ion beam (Ar^+ sputtering) and electron beam (during AES measurements).

3. Results

3.1. Sodium metal

The native sodium metal samples were always covered by thin reaction layers containing mixed oxides, carbonates and possibly fluorides. The pure metallic state of sodium could never be observed immediately.

Fig. 1 presents results of XPS measurements of three sample states: as coming from the glove box (black), sputter-treated with Ar^+ ions (red) and in situ scraped (blue). To demonstrate the above discussed peak overlays with the Na-KLL Auger lines depending on Al-Kα or Mg-Kα X-ray excitation, the Na1s, C1s and O1s spectra are plotted for both X-ray excitations. Here, the disturbing peaks in the C1s (Mg-Kα) and O1s (Al-Kα) spectral windows are visible and marked with arrows. In Na1s, only the broadening in the spectra by the larger line width of the non-monochromatized Mg-Kα radiation is visible. In the following figures for these spectral windows, only the undisturbed spectral data are considered: Na1s and C1s measured with Al-Kα and O1s measured with Mg-Kα radiation. The stoichiometry estimations, therefore, are always done only for Na:C (Al-Kα) and Na:O (Mg-Kα).

The sample from the box clearly contains oxygen species (the ratio Na:O = 47:53). After scraping, only traces of O were found (Na:O=96:4). Also, the carbon concentration confirms this trend: box (Na:C= 47:53); scraped (Na:C = 99.5:0.5). The values for sputter-cleaning are in between these values. Further contaminations from F and K are below 0.5 and 1 at%, respectively, when surface cleaning with scraping was applied.

In the Na1s (a1, a2) spectra, the oxidized state (black) is characterized by a shift to higher BE and a broader peak at 1074 eV, the scraped metallic state (blue) shows a sharp peak at 1072 eV and strong plasmon loss peaks while the sputtered state shows a mixture of both. In the C1s spectra measured with Al-Kα (b1) coming from the box (black), the two main carbon contamination peaks at 293 eV (carbonate) and 288 eV (C-H and C-C) are shifted around 3 eV to higher BE with respect to their standard positions (red arrows), as previously observed for Li and K. The mentioned Na1s position at 1074 eV for the oxide-like species is similarly shifted to higher BE in comparison with the peak position with the commonly used BE referencing using the C-H contamination peak at 285 eV [22]. During sputtering (red), an additional peak in standard position at 285 eV originates from carbon species being in the direct contact with the Na metal. After scraping (blue), the peak of remaining carbon is still at the high position of about 287.5 eV, obviously still present at the surface of Na-oxide residuals. The small peak doublet at around 294/296 eV is originating from the small amount of residual potassium present in the sodium material in order of less than 1 at%. The broad O1s peak (c2) in the sample from the glove box points to a mixed oxide state, presumably carbonate and oxide/hydroxide. During sputtering, an O1s peak (blue arrow) at low BE position of 530 eV is formed, characteristic for an overlayer conversion to Na_2O.

In summary, the metal samples prepared in the glove box were covered by a mixture of (hydr-) oxide with a small amount of carbonate, which is damaged during Ar^+ sputtering.

In Fig. 2, the peak maxima for the C1s (a), O1s (b), Na1s (c) and Ar2p (d) positions are plotted as an overview for better comparison of several reaction layers found at the metallic sample. The three states from Fig. 1 (from the glove box - A, from the glove box and sputtered - B, after scraping - C) are extended for comparison with the states “scraped and sputtered” - D, “in contact with air” - E, “contact with air and sputtered” – F. These sample states generally confirm the conclusions made with Fig. 1. The metallic state after sputtering (D) is characterized by the strong plasmon loss peaks (Pl), and after sputtering the residual contamination tends to be transferred into Na_2O with O1s at 530 eV. After contact with air (E), a strong C1s peak at 293 eV (Fig. 2a) and one dominating O1s peak at around 534 eV (Fig. 2b) point to formation of relatively pure sodium carbonate Na_2CO_3. The estimated stoichiometry with Na:C = 68:32 and Na:O = 43:57 also supports this assumption. This agrees with the observation of pure carbonate formation for Li and K when being in contact with air. Sputtering with Ar^+ (F) leads to decomposition of the carbonate here as well: a small second O1s peak at 530 eV, corresponding to the Na_2O position (Fig. 2b) appears, and a lowering of the O concentration is observed. Implanted Ar from the sputtering process is found for all sputter treated samples, Na-metal from the box (B), Na-metal scraped (D) and after contact with air (F) with the Ar2p peak position at 246 eV (Fig. 2d), also at a higher BE position, as previously observed also for Li and K.

The formation of passivation layers at the sodium surface in air is assumed from the chemical point of view [22] to be stepwise from sodium (hydr)oxide (NaO_y - NaOH) to sodium hydrogencarbonate $NaHCO_3$ and/or sodium carbonate Na_2CO_3. The observation of minor chemical shifts in O1s and Na1s [22,33,34] makes the differentiation between the several species complicated. Therefore, in Fig. 2, two self-prepared reference carbonate layers (“from air” - E, and “from air and sputtered” - F) are additionally compared with a not-precleaned metal sample coming from the glove box after 10 s in contact with air “box and air” (G - from [22]) and a commercial $NaHCO_3$ (MERCK, p.a.) powder (H). It has to be noted that the last two samples showed BE shifts from charging (thick insulating materials) and a BE correction was done with respect to the C1s carbonate position from the first two not-charging sample states (E, F). There are no significant peak shifts between the four samples (G-F) found, also not in the O1s peaks, which would be assumed for conversion from NaOH to $Na(H)CO_3$.

For further information, we looked also at the calculated stoichiometries from the XP spectra. Although there are possible uncertainties coming from lateral and in-depth inhomogeneity of the surface layers, the comparison of the measuring results with the nominal stoichiometries can be helpful. Table 1 shows the calculated Na:C (carbonate-part) concentrations (from Al-Kα measurements) and the Na:O concentrations (from Mg-Kα measurements) in comparison with the nominal ratios for pure compounds. Especially the Na:C ratios confirm that no pure sodium hydrogen carbonate was formed. The reference $NaHCO_3$ compounds also contains rather Na_2CO_3 on the surface. Obviously, at all the surfaces (clean Na-metal, Na-metal from the glove box, and commercial $NaHCO_3$) after contact with air, predominantly carbonate was found. For the clean metal sample after air contact, the observed stoichiometry matches almost perfectly with Na_2CO_3.

Measurements with AES in the JEOL JAMP-9500 system were intended on testing the possibilities of this method for local analysis of the Na-containing samples. Thus, as in the previous studies for Li and K material [14,15], area-dependent investigations are in the focus. Fig. 3 shows secondary electron (SE) pictures of three different Na-metal

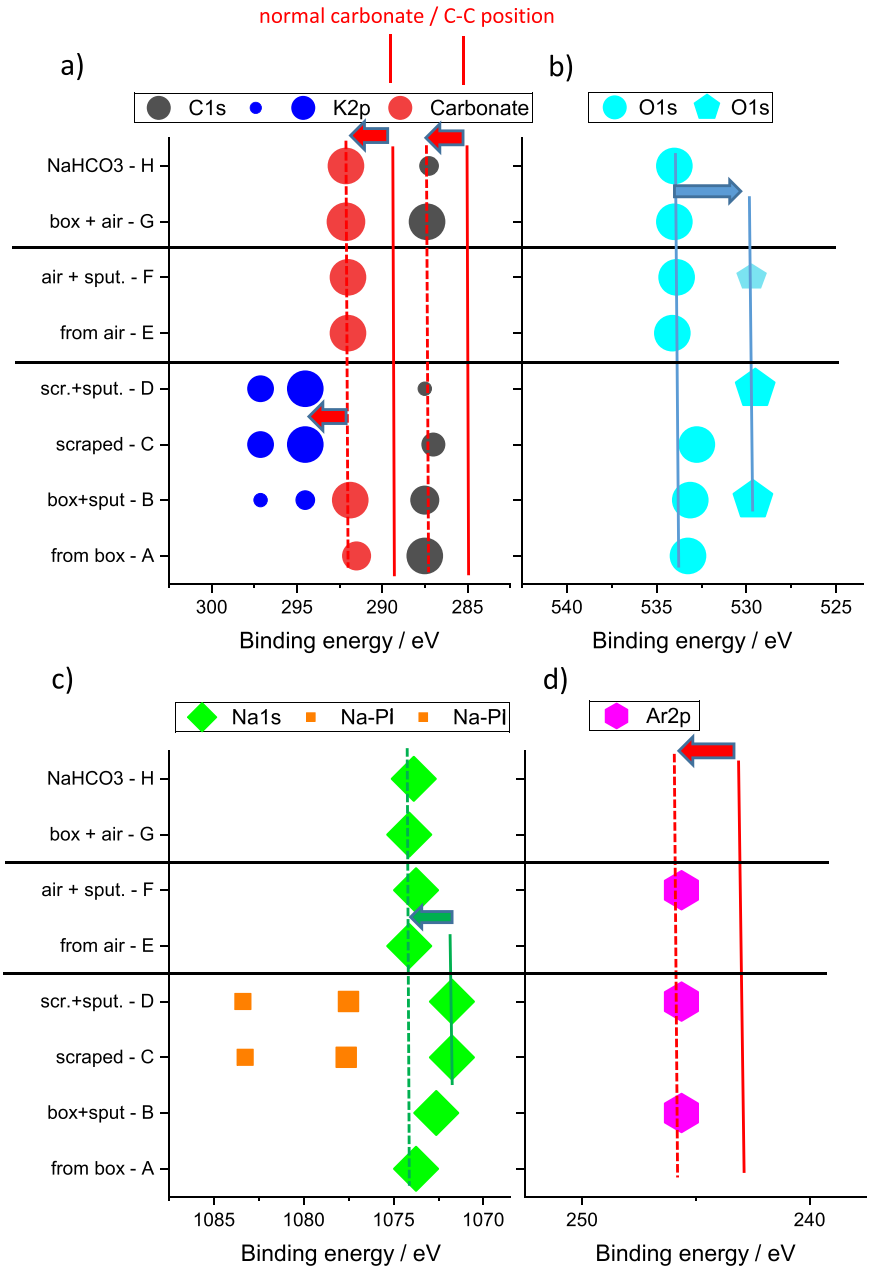

Fig. 2. Plot of the peak maxima at the BE scale detected with XPS measurements for several states of metallic Na samples and the $NaHCO_3$ reference material; detailed explanation is given in the text. Different size of the symbols qualitatively shows intensity variations. The red arrows point to the 3 eV BE shift of overlayers and sputter-implanted Ar induced by the potential barrier for samples with high Na concentration. The blue arrow symbolizes the oxide decomposition during sputtering. The green arrow shows the BE peak shift for Na1s from Na metal to Na oxide overlayers, Na-Pl shows the position of the plasmon peaks occurring for metallic Na.

samples under investigation: as coming from the glove box (a, b), after contact with air (c, d) and after cleaning by in situ scraping (e). In general, the samples, which are covered with oxide layers (a, c), are relatively rough, only the scraped surface (e) appears smooth. In particular, the sample coming from air (c, d) shows a microscopic cauliflower-like structure. In the left part (a, c, e), the applied measuring areas are marked in red. The SE pictures after the AES measurements (b, d) show drastic changes for the medium and local analysis areas; for the scraped sample no changes were observed (not shown). The observation time used was 8 min of electron beam exposure (10 nA @ 10 keV) for each area. This observation points to the assumption that a massive destruction of the surface layers is caused by the electron beam.

This assumption was confirmed by AE spectra shown in Fig. 4, where the results from large area and spot measurements for several samples are compared. The observed intensities of CKLL (b) and OKLL (c) peaks at the large measurement area of the samples covered with carbonate-like overlayers (from box - black, from air - blue) are clearly decreasing for the appropriate spot measurements (red, green) already after the relatively short measuring time of 8 min. Certainly, the carbonate-like species are converted to oxides. At the scraped surface (b, c), no C and O was found and no changes occurred during AE measurement.

With the XPS method, the chemical nature of the overlayers formed could be clearly classified: mixed oxide/carbonate when coming from the glove box, nearly pure carbonate after contact with air. Ar^+ sputtering led to decomposition of the observed surface oxide species. The

Table 1
Stoichiometry ratios of samples from Fig. 2 (E,F,G,H) in comparison with the nominal ratios for the expected standard compounds. The Na: C and Na: O ratios were estimated from separate XPS measurement with Al-Kα and Mg-Kα radiation. The results point mainly to carbonate formation at the Na surfaces.

Sample	in Fig. 2	Na: C	Na: O	comment
clean metal on air	***E***	72: 28	46: 54	nearly Na_2CO_3
from air and Ar^+ sputtering	***F***	82: 18	53: 47	C and O loss from sputtering
from box 10 s air	***G***	77: 23	33: 67	not clear $NaHCO_3$, NaOH residuals
$NaHCO_3$ - reference powder	***H***	63: 37	36: 64	near to Na_2CO_3
nominal Na_2O		100: 0	67: 33	should also show a separate O1s peak
nominal NaOH		100: 0	50: 50	
nominal Na_2CO_3		67: 33	40: 60	
nominal $NaHCO_3$		50: 50	25: 75	

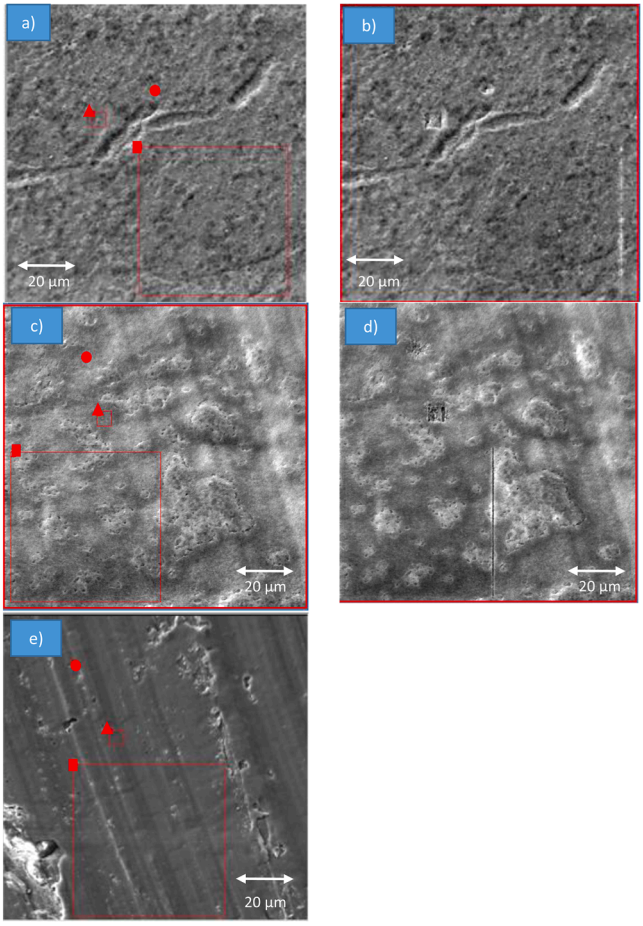

Fig. 3. Secondary electron (SE) pictures (size 100 µm x 100 µm) for metallic Na samples coming from glove box (a, b), after contact with air (c, d) and after in situ scraping (e). In the left pictures (a, c, e) before the AES measurement the measuring areas are marked (1 - 50 µm x 50 µm, 2 – 5 µm x 5 µm, 3 - spot), in the right pictures (b, d) morphology changes point to destruction of overlayer material by the electron impact during the measurements.

AES investigations point to very rough surface layers, which are strongly modified by the electron beam. Thus, with the AES method, the identification of the elements at the surfaces is possible, however, the chemical information is poor due to beam damage.

3.2. *Intercalated graphite*

For both Li and K, a full intercalation was found during our previous investigations [14,15], for the exfoliated HOPG surfaces, the stoichiometry results from XPS represent LiC_6 [35] and $KC_{\sim 8}$ [36]. For Na intercalation, there is no clear evidence in the literature, pointing that intercalation of significant amount of Na into graphite could not be realized. The only battery-relevant electrochemical insertion of sodium into graphite represents a co-intercalation of Na-coordinating molecules from the electrolyte solvent (e.g. [29]).

For our surface analytical reference measurements to look for interaction/reaction of Na with graphite, we therefore tried different preparation methods:

- a thermal intercalation, which was successful for Li and K [14,15],
- electrochemical co-intercalation in an electrochemical cell, similar to [29],
- *in situ* Na deposition in a preparation chamber.

Similar to Fig. 2 for the Na-metal samples, Fig. 5 shows for a series of Na-treated HOPG samples the peak maxima observed with XPS for the C1s (a), O1s (b), Na1s (c), F1s (d), Ar2p (e), and S2p (f) spectra as an overview. Table 2 summarizes the estimated elemental concentrations for all these species.

The C1s peak for HOPG is mostly not changed in position in all the experiments, beside a small broadening from an interaction with the surface species. For Li and K, there was a peak shift (and partly an asymmetry) observed in our previous works after intercalation.

3.2.1. *Thermal intercalation*

For the thermal intercalation, four states are compared in Fig. 5 for Na-treated HOPG samples after in situ delamination. Different surface concentrations of Na were found depending on variation of the used delaminated areas:

A) native HOPG,
B) area with a low Na amount (10 at%),
C) area with a low Na amount (10 at%) and sputtering,
D) area with a high Na amount (40 at%) and sputtering.

In all investigated areas, oxygen and fluorine were found, pointing to oxide and oxyfluoride species in the sample. In the C1s spectra, hints for carbonate residuals were also found. The C1s peak is broadened in comparison to the HOPG, Na is at the oxide-containing position (see Fig. 1) at around 1073 eV. F1s is found mainly at a low BE position (685-686 eV) and, when coming from the glove box, with lower intensity at a high BE position (688-689 eV). The high BE part is attributed to an F-O containing species, because it decreased after sputtering parallel to decrease of the O content. In all our delamination experiments, we never found areas completely free of oxygen. The BE position of the Ar2p peak varies with the Na content from low (C) to high (D) position (242 - 246 eV), obviously being a mixture of implantation into Na-pure and Na-rich areas.

This delaminated HOPG sample area was investigated subsequently after Ar-transfer from the XPS system also in the AES system. In Fig. 6, the results are presented. The SE picture confirms a flat surface from graphite layer delamination in the XPS system, some particles are locally visible. AES spectra are shown for 3 measuring areas of different size: area1 - 100 × 100 µm (black), area2 - 10 × 10 µm (red), area3 - spot 100 nm diameter (blue). Electron beam exposure time here was 10 min for

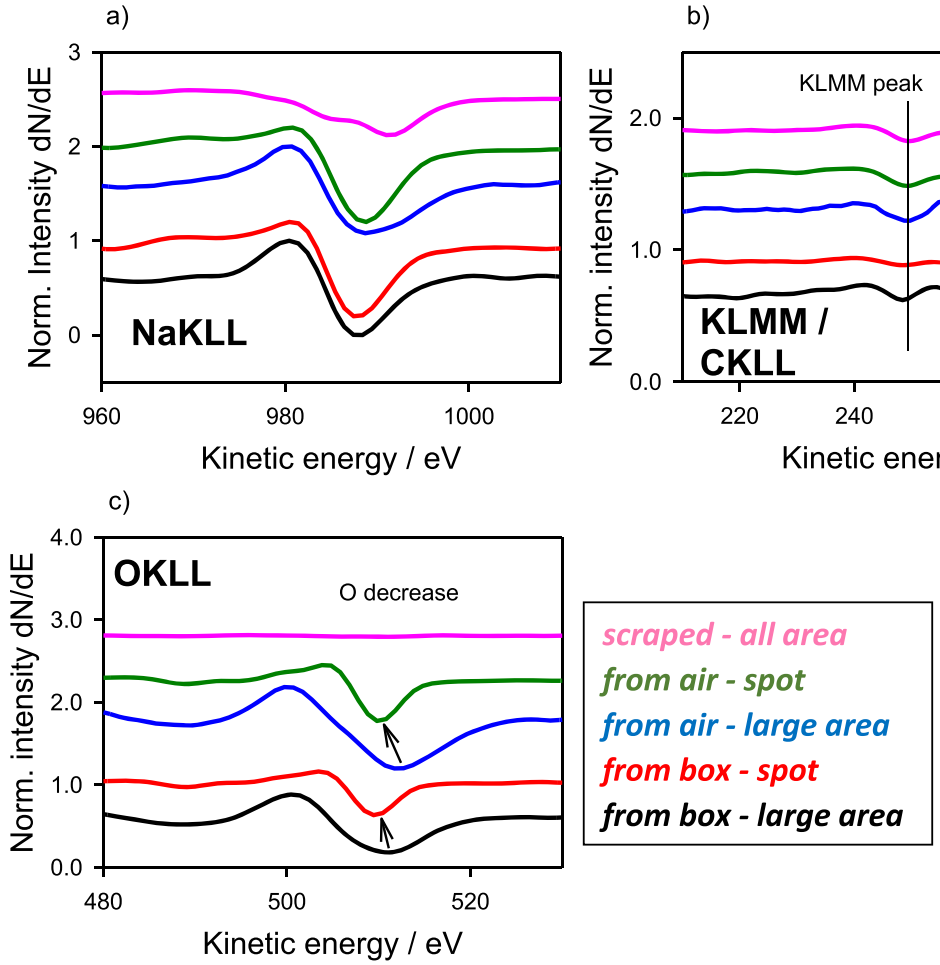

Fig. 4. Differentiated NaKLL (a), CKLL (with KLLM side peak - b) and OKLL (c) AES spectra normalized to Na KLL intensity for Na metal samples coming from glove box (black, red), after contact with air (blue, green) and after in situ scaping (violet). As suspected from the secondary electron pictures shown in Fig. 3 the spectra for the spot measurements show with C and O loss a decomposition of the overlayer material (black to red, blue to green). The clean metallic state (violet: no O, no C) is characterized by a specific NaKLL peak shape.

each area. With smaller areas, the F content is decreasing, and in the CKLL spectra a shift from 260 to 270 eV is visible, OKLL is decreasing only slightly. This agrees with the previous observations: fluorine species are damaged by ion beam while carbonates are known to be destroyed by electron beam (see Fig. 4).

With the AES maps shown in Fig. 7, it is confirmed that the particles described already with Fig. 6 are precipitated Na-oxide species.

Delamination experiments were also done in the AES analysis system. There, mostly as in the XPS investigations, only Na in combination with oxygen (and partly fluorine) was observed. After several delamination treatments, also deeper regions of the HOPG could be prepared, where locally no Na was detected.

From all these results, it becomes clear that no complete thermal insertion of Na into the graphite was possible. In combination with the XPS results we conclude that Na, which we attempted to intercalate by the thermochemical procedure, is always in mixed oxide-like state.

3.2.2. *Electrochemical intercalation*

For the electrochemical intercalation, three states are compared in Fig. 5:

E) - electrochemical intercalated HOPG as coming from glove box,
F) - electrochemical intercalated HOPG delaminated in the XPS system,
G) - electrochemical intercalated HOPG delaminated and Ar^+-sputtered.

The sample from the glove box (E) is obviously completely covered by residuals of the chemicals dissolved in the electrolyte. Thus, in the C1s spectra of this sample nearly no peak from the HOPG substrate (285 eV) is visible, the spectrum is dominated by C-O (288 eV) and C-F (294 eV) bonded carbon. The high BE peak for S2p (172 eV) points to S-O bonding in oxidized S-species, the two peaks at F1s (686 and 691 eV) could be attributed to Na-F and C-F bonds. A minor chlorine contamination is found at the surface. After first delamination (F) the C1s peak for graphite is visible, while the other peak positions are in general not changed. During sputtering of a 5 nm in-depth equivalent (G), the C-F bindings were destroyed, and the S-species were reduced, while Na-F species did not change. After several delamination procedures in the deeper regions of HOPG, the part of Na in oxide-like Na-species increased, but no sign of element-like Na was found. All this is also confirmed by the estimated element concentration given in Table 2.

These results confirm the assumption (see e.g. [29]) that the observed reversible electrochemical activity in not the result of a direct reaction of elemental Na with the graphite, but is due to the reversible (co-)intercalation of the Na-containing molecules.

3.2.3. *In situ deposition*

For *in situ* Na deposition, three states are compared in Fig. 5:

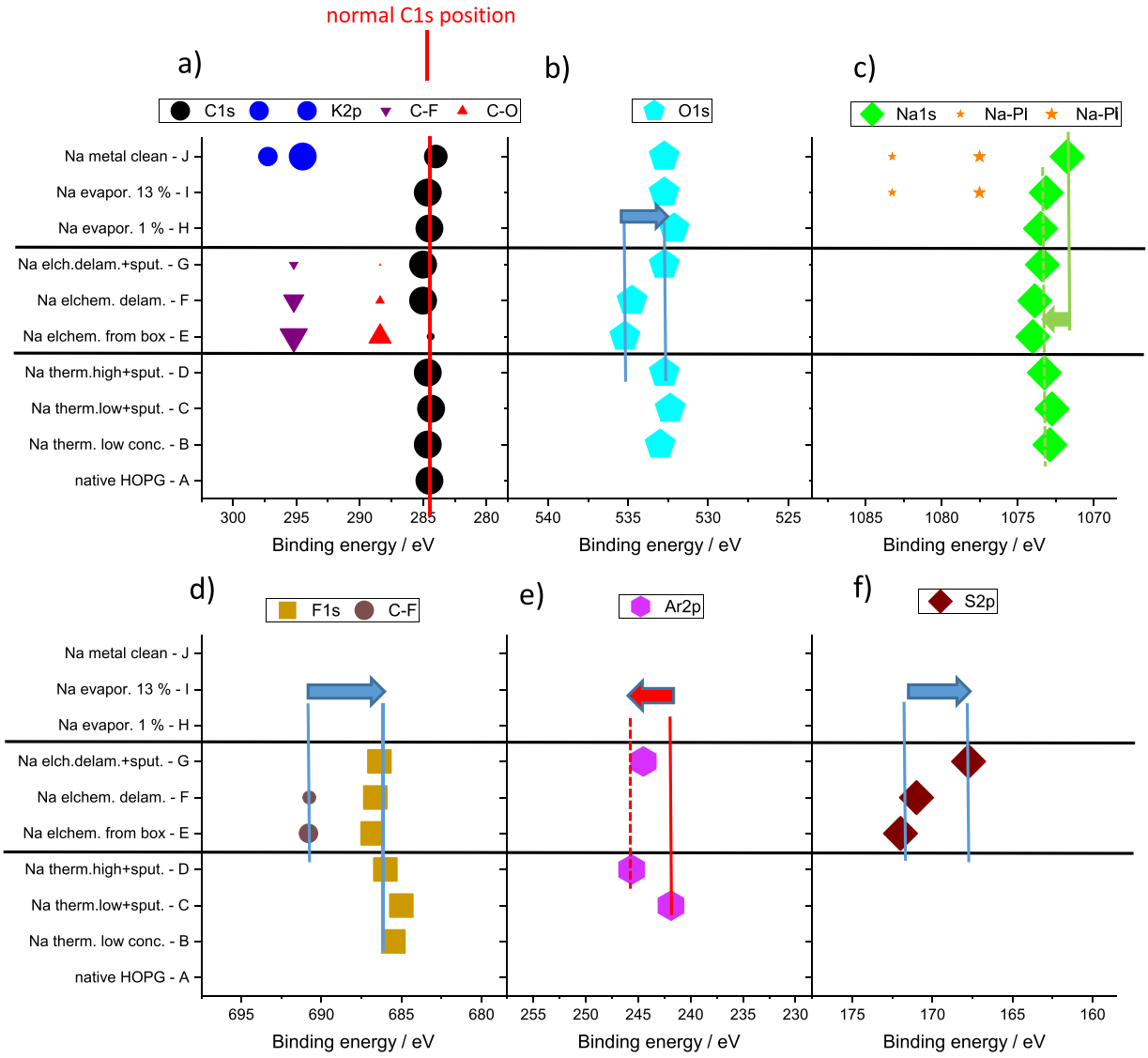

Fig. 5. Plot of the peak maxima at the BE scale detected with XPS measurements for several states of HOPG samples after treatment with Na and reference material - detailed explanation is given in the text. Different size of the symbols qualitatively shows intensity variation. The red arrows point to the 3 eV BE shift of overlayers and sputter-implanted Ar induced by the potential barrier for samples with high Na concentration. The blue arrows symbolize the damaging of oxide species during sputtering. The green arrow shows the BE peak shift for Na1s from Na metal to Na oxide overlayers. The C1s peak is always in the standard C-C position for HOPG. For the samples from electrochemical treatment additional peaks for C-F and C-O species were observed.

Table 2
Estimated surface concentrations for the HOPG samples shown in Fig. 5 For thermal preparation O and F is found, depressed by sputtering. For the electrochemical preparation also after delamination the species from the electrolyte (F, S, Cl) always are found. The high amount of Na at the surface for in situ deposition points to layer formation at the HOPG surface - no intercalation.

Sample state	preparation	C	Na	O	Ar	F	S	Cl	in Fig. 5
HOPG	native	100	0	0	0	0	0	0	***A***
box -low Na	thermal	82	10	5	0	3	0	0	***B***
low Na + sput	thermal	86	10	1	2	1	0	0	***C***
high + sput	thermal	51	41	3	1	4	0	0	***D***
from box	electrochemical	13	29	22	0	28	4	3	***E***
delamination	electrochemical	30	23	19	0	21	4	2	***F***
del.+ sputtering	electrochemical	29	38	8	0	23	0.5	0	***G***
1 % Na	deposition	97	1	2	0	0	0	0	***H***
13 % Na	deposition	84	13	3	0	0	0	0	***I***
Na-pure	scraped	2	95	3	0	0	0	0	***J***

H) - HOPG with 1 at% Na (0.5 min deposition),
I) - HOPG with 13 at% Na (8 min deposition),
J) - metallic Na (after scraping).

In the C1s peaks for the different deposition steps with increasing Na concentration a small asymmetric broadening is observed. The O1s peaks from oxygen imbedded from the residual gas in the preparation

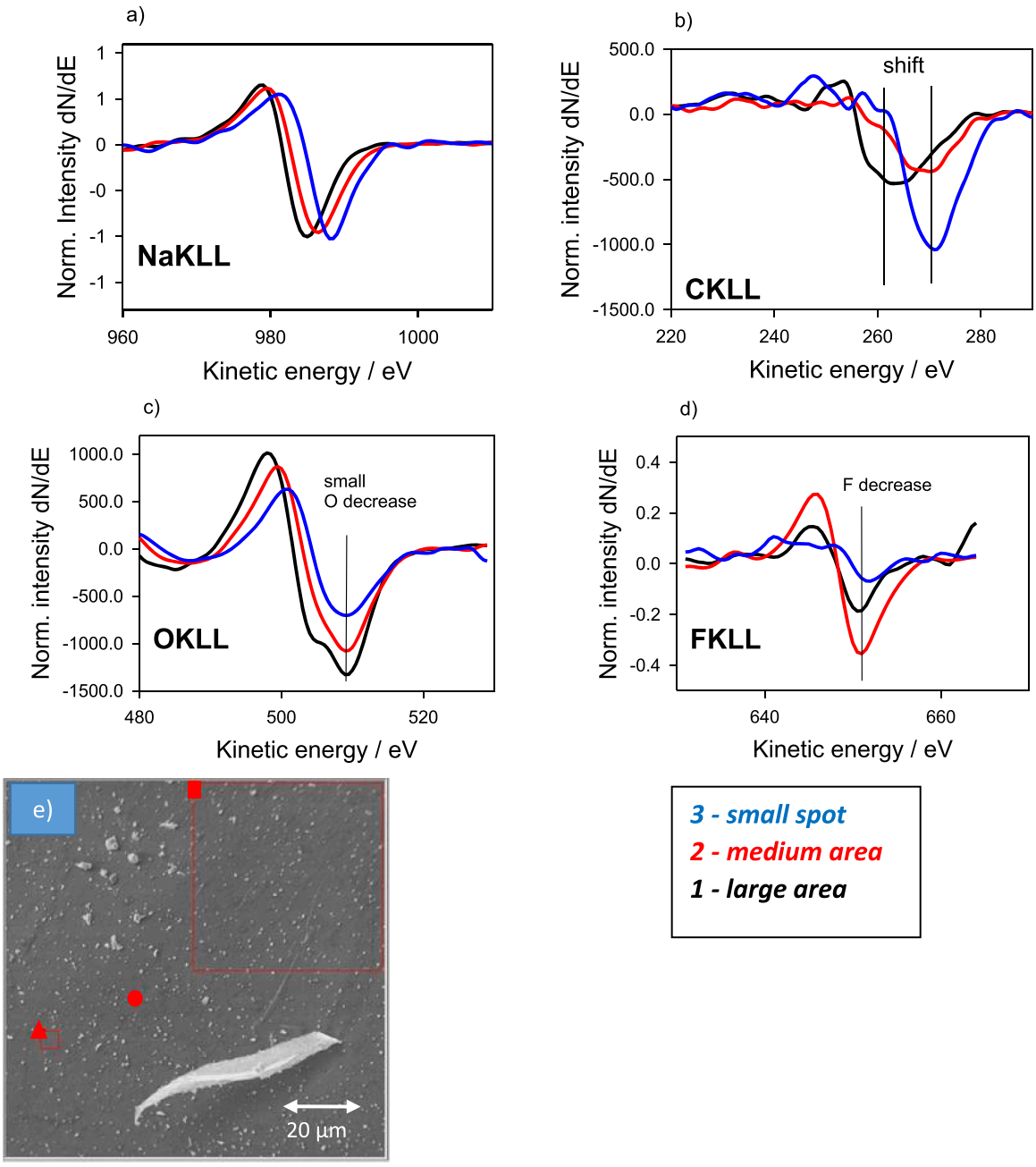

Fig. 6. AES spectra (a, b, c, d) for the thermally intercalated HOPG sample delaminated in the XPS system normalized to similar NaKLL peak height (a) for three different measuring areas (1- 50 µm x 50 µm, 2 - 5 µm x 5 µm, 3 - spot) shown in the SE picture with the size 100 µm x 100 µm (e) . With decreasing of the measuring area mainly F is decreasing - as observed while sputtering (Tab. 2) the fluorine compounds are decomposed also due to electron impact. At the SE picture (e) small particles at the smooth delaminated surface are clearly visible.

chamber are in intermediate BE position (at around 532.5 eV); the relative O concentration is stepwise decreased with Na deposition - O: Na ratio changing from 60: 40, via 40: 60 to 20: 80, see also Table 2. The Na1s peak is for low Na amount (H) in oxide position (1073 eV), for the highest Na amount (I) a broadening to the Na metal low BE position is observed, similarly the small plasmon loss peaks (Pl) point to beginning metallic character of the deposited Na material.

In conclusion these phenomena point to a step-by-step deposition of sodium on top of the HOPG, not to an intercalation. If an intercalation of elemental Na would take place, due to the in-depth diffusion a concentration saturation of Na at a low concentration level should be observed and Na should not be found in metallic state.

4. Summary and conclusion

The observations made with XPS for metallic Na samples are very similar to that previously found in out investigations for metallic Li and K samples. The main result is a 3 eV spectral shift to higher BE's for insulating species when they are in contact with surfaces highly enriched with the alkaline elements (Li, K, Na). This effect is important for the correct interpretation of chemical species in battery materials. These BE shifts we interpret as the result of a "potential barrier", which is induced by an interface dipole layer. Recently we discussed this interface dipole in relation to the chemical standard electrode potentials of the alkaline elements [37], when assuming a complete local ionization of the insulating overlayer. Especially in case of surface charging,

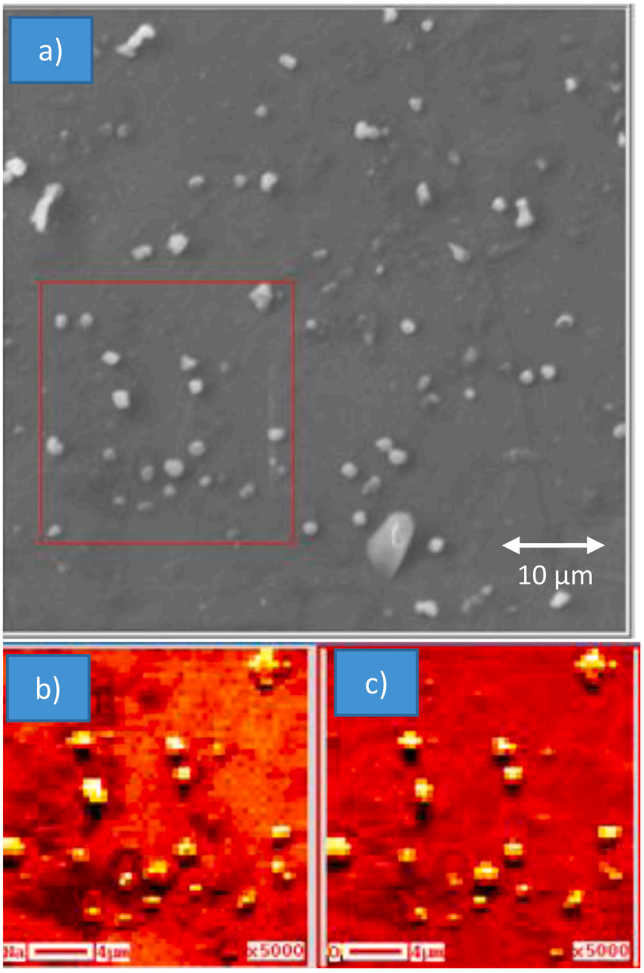

Fig. 7. AES intensity maps for Na (b) and O (c) of the delaminated HOPG surface from thermal intercalation. The AES measuring region (size 24 µm x 24 µm) is marked with a red rectangle in the SE picture (a) - size 60 µm x 60 µm. The particles found at the surface are obviously Na-O type precipitates.

when the common approximation of BE correction using the C1s peak position at around 285 eV is applied, the possible shift to higher energies due to the interface dipole must be necessarily taken into account. For the correct estimation of element concentrations and also for the chemical species identification at the surface, XPS measurements should be done using combination of both, Al- and Mg-Kα X-rays in separate measurements, due to the mentioned peak-overlay of the O1s and C1s peaks with Na-KLL lines. Such complication is not occurring for the XPS investigations of Li or K.

In general, the reaction layers formed at the metal Na surfaces showed much more roughness then previously observed for Li and K, which could point to a much higher reactivity of sodium. The identification of complex surface species like Na-(hydro)carbonate or -hydroxide, expected from chemical point of view, is less straightforward in comparison to Li and K components due to the insufficient spectral differences (tiny BE shifts) between them. Some cross contaminations with K and F were found. As the final reaction product between metallic Na and air components, Na_2CO_3 was always detected. This carbonate formation is in agreement with our observations made for Li and K.

Although AES investigations can be used for the local identification of surface elements at the metallic samples, electron beam damage, however, restricts the chemical information. Also, Ar^+ sputtering used for surface cleaning leads to decomposition of the chemical species such as carbonate or fluorides at the surfaces.

As expected from previous investigations, Na-ions cannot be inserted into graphite, neither electrochemically nor via chemical reaction at elevated temperatures. The temperature-induced alkali metal intercalation into HOPG was clearly shown for Li and K in our previous XPS investigations, performed under similar conditions. Using a thermal intercalation process only (predominantly localized), Na-oxide type species were found after the *in situ* delamination of surface reaction layers. For the electrochemical co-intercalation of Na-ions with the solvent molecules, which is discussed as applicable for Na-batteries, always only the reaction products with the electrolytes were found. In situ evaporation of Na directly in the vacuum chambers only led to deposition of various Na-species on top of the graphite and not to a real intercalation. For higher Na surface concentrations, even Na in metallic state could be observed.

The AES method is mostly focused to local spatial analysis. In our investigations we could visualize local Na-oxide type precipitations at the HOPG. As in the case of other alkali metals, the electron beam led to decomposition of the oxide-like surface species, especially for small spot analysis. For typical conditions necessary for sufficient signal-to-noise ratios (here 10 nA @ 10 keV), only measuring time below one minute is acceptable for spot analysis. In summary, the XPS method is favorable for chemical investigation at alkali-dominated surfaces when large area information is sufficient. Despite of the mentioned beam damage effects, however, AES can complement the XPS results with local information while carefully controlling the used energy dose.

In conclusion, despite using nearly ideal preparation and analysis conditions for our model systems, the obtained results are viable for the application of electron spectroscopy methods also for metal-ion battery materials concerning both, proper BE definition for the measured spectra and possible beam damage during analysis.

Funding

This work was supported by the Bundesministerium für Bildung und Forschung (BMBF), project number 03XP0390C, and by the German Research Foundation (DFG), project number 448719339.

CRediT authorship contribution statement

S. Oswald: Writing – review & editing, Writing – original draft, Methodology, Investigation, Formal analysis, Conceptualization. **A. Thomas:** Writing – review & editing, Visualization, Investigation. **M.V. Gorbunov:** Writing – review & editing, Investigation. **D. Mikhailova:** Writing – review & editing, Project administration, Funding acquisition, Conceptualization.

Declaration of competing interest

The authors declare that they have no known competing financial interests or personal relationships that could have appeared to influence the work reported in this paper.

Acknowledgments

The authors are indebted to S. Kaschube (IFW Dresden) for assistance with the cleaving and scraping experiments in the analysis systems, A. Voss and A. Voidel (both IFW Dresden) for performing ICP-OES analysis. M. Hantusch (IFW Dresden) was involved into the Na *in situ* deposition experiments and the data treatment for some of the figures.

Supplementary materials

Supplementary material associated with this article can be found, in the online version, at doi:10.1016/j.surfin.2026.108427.

Data availability

The authors do not have permission to share data.

References

[1] T. Kim, W. Song, D.-J. Son, L.K. Ono, Y. Qi, Lithium-ion batteries: outlook on present, future, and hybridized technologies, J. Mater. Chem. A 7 (2019) 2942–2964.

[2] Y. Tian, G. Zeng, A. Rutt, T. Shi, H. Kim, J. Wang, J. Koettgen, Y. Sun, B. Ouyang, T. Chen, Z. Lun, Z. Rong, K. Persson, G. Ceder, Promises and Challenges of Next-Generation "Beyond Li-ion" Batteries for Electric Vehicles and Grid Decarbonization, Chem. Rev. 121 (2021) 1623–1669.

[3] H. Zhang, S. Zhao, F. Huang, A comparative overview of carbon anodes for nonaqueous alkali metal-ion batteries, J. Mater. Chem. A 9 (2021) 27140.

[4] S. Sunny, S. Suriyakumar, A.S. Sajeevan, Strategies to develop stable alkali metal anodes for rechargeable batteries, J. Phys. Energy 6 (2024) 022004.

[5] A. van der Ven, Z. Deng, S. Banerjee, S.P. Ong, Rechargeable Alkali-Ion Battery Materials: Theory and Computation, Chem. Rev. 120 (2020) 6977–7019.

[6] P. Verma, P. Maire, P. Novák, A review of the features and analyses of the solid electrolyte interphase in Li-ion batteries, Electrochim. Acta 55 (2010) 6332–6341.

[7] E. Peled, S. Menkin, Review – SEI: past, present and future, J. Electrochem. Soc. 164 (2017) A1703–A1719.

[8] C.-Y. Tang, K. Leung, R.T. Haasch, S.J. Dillon, $LiMn_2O_4$ Surface Chemistry Evolution during Cycling Revealed by in Situ Auger Electron Spectroscopy and X-ray Photoelectron Spectroscopy, ACS Appl. Mater. Interfaces 9 (2017) 33968–33978.

[9] C.Y. Tang, L. Feng L, R.T. Haasch, S.J. Dillon, Surface redox on $Li[Ni_{1/3}Mn_{1/3}Co_{1/3}]O_2$ characterized by in situ X-ray photoelectron spectroscopy and in situ Auger electron spectroscopy, Electrochimica Acta 277 (2018) 197–204.

[10] K.N. Wood, G. Teeter, XPS on Li-Battery-Related Compounds: Analysis of Inorganic SEI Phases and a Methodology for Charge Correction, ACS Appl. Energy Mater. 1 (2018) 4493–4504.

[11] S. Oswald, Binding energy referencing for XPS in alkali metal-based battery materials research (I): Basic model investigations, Appl. Surf. Sci. 351 (2015) 492–503.

[12] S. Oswald, F. Thoss, M. Zier, M. Hoffmann, T. Jaumann, M. Herklotz, K. Nikolowski, F. Scheiba, M. Kohl, L. Giebeler, D. Mikhailova, H. Ehrenberg, Binding Energy Referencing for XPS in Alkali Metal-Based Battery Materials Research (II): Application to Complex Composite Electrodes, Batteries 4 (2018) 36.

[13] S. Oswald, Auger- and X-ray Photoelectron Spectroscopy at Metallic Li Material: Chemical Shifts Related to Sample Preparation, Gas Atmosphere, and Ion and Electron Beam Effects, Batteries 8 (2022) 24.

[14] S. Oswald, T. Schmeida, D. Mikhailova, Model experiments with Auger electron and X-ray photoelectron spectroscopy at lithiated graphite material: chemical shifts related to ion- and electron-beam effects, Appl. Surf. Sci. 619 (2023) 156776.

[15] S. Oswald, M.V. Gorbunov, D. Mikhailova, Electron spectroscopy investigations of potassium and potassium-intercalated graphite with battery background, Appl. Surf. Sci. 655 (2024) 159614.

[16] M.C. Biesinger, Accessing the robustness of adventitious carbon for charge referencing (correction) purposes in XPS analysis: Insights from a multi-user facility data review, Applied Surf. Sci. 597 (2022) 153681.

[17] J. Maibach, F. Lindgren, H. Eriksson, K. Edström, M. Hahlin, Electric Potential Gradient at the Buried Interface between Lithium-Ion Battery Electrodes and the SEI Observed Using Photoelectron Spectroscopy, J. Phys. Chem. Lett. 7 (2016) 1775–1780.

[18] H. Okamoto, Li-O (Lithium-Oxygen), J. of Phase Equilibria and Diffusion 34 (2013) 2.

[19] Y. Li, Q. Liu, S. Wu, L. Geng, J. Popovic, Y. Li, Z. Chen, H. Wang, Y. Wang, T. Dai, Y. Yang, H. Sun, Y. Lu, L. Zhang, Y. Tang, R. Xiao, H. Li, L. Chen, J. Maier, J. Huang, Y.-S. Hu, Unraveling the Reaction Mystery of Li and Na with Dry Air, J. Am. Chem. Soc. 145 (2023) 10576–10583.

[20] H. Okamoto, K-O (Potassium - oxygen), J. of Phase Equilibria 19 (1998) 4.

[21] J. Sangster, K-O (Potassium-Oxygen) System, J. of Phase Equilibria and Diffusion 34 (2013) 1.

[22] A. Thomas, B. Pohle, J. Schultz, M. Hantusch, D. Mikhailova, NaOH protective layer for a stable sodium metal anode in liquid electrolytes, Journal of Energy Storage 77 (2024) 109900.

[23] R.C. Asher, A lamellar compound of sodium and graphite, J. Inorg. Nucl. Chem. 10 (3-4) (1959) 238–249.

[24] H.L. Recht, G.M. Wolten, D.E. Gilmartin, The interaction of graphite with sodium-vapor, J. Inorg. Nucl. Chem. 23 (3-4) (1961) 275–278.

[25] P. Ge, M. Fouletier, Electrochemical intercalation of sodium in graphite, Solid State Ionics 28-30 (1988) 1172–1175.

[26] I.A. Udod, H.B. Orman, V.K. Genchel, The sodium-graphite system under high pressure conditions: the comparison with the lithium-graphite system, Carbon 32 (1994) 101–106.

[27] H. Moriwake, A. Kuwabara, C.A.J. Fisher, Y. Ikuhara, Why is sodium-intercalated graphite unstable? RSC Adv. 7 (2017) 36550.

[28] F. Wang, Z. Jiang, Y. Zhang, Y. Zhang, J. Li, H. Wang, Y. Jiang, G. Xing, H. Liu, Y. Tang, Revitalizing sodium-ion batteries via controllable microstructures and advanced electrolytes for hard carbon, eScience 4 (2024) 100181.

[29] B. Jache, P. Adelhelm, Use of Graphite as a Highly Reversible Electrode with Superior Cycle Life for Sodium-Ion Batteries by Making Use of Co-Intercalation Phenomena, Angew. Chem. Int. Ed. 53 (2014) 10169–10173.

[30] M. Goktas, C. Bolli, E.J. Berg, P. Novák, K. Pollok, F. Langenhorst, M. Roeder, O. v. Lenchuk, D. Mollenhauer, P. Adelhelm, Graphite as Cointercalation Electrode for Sodium-Ion Batteries: Electrode Dynamics and the Missing Solid Electrolyte Interphase (SEI), Adv. Energy Mater. 8 (2018) 1702724.

[31] J.H. Rhee, B. Ha, S.C. Sharma, Electronic structure and electrical properties of Na-doped C_{60} thin films, Thin Solid Films 517 (2008) 522–524.

[32] D. Pontiroli, S. Scaravonati, M. Sidoli, G. Magnani, L. Fornasini, C. Milanese, M. Riccò, Fullerene mixtures as negative electrodes in innovative Na-ion batteries, Chemical Physics Letters 731 (2019) 136607.

[33] P.H. Citrin, High-Resolution X-Ray Photoemission from Sodium Metal and Its Hydroxide, Phys. Rev. B 8 (1973) 5545–5556.

[34] A. Barrie, F.J. Street, An Auger and X-ray photoelectron spectroscopic study of sodium metal and sodium oxide, J. Electron Spectrosc. Rel. Phenom. 7 (1975) l–31.

[35] D. Guerard, A. Herold, Intercalation of lithium into graphite and other carbons, Carbon 13 (1975) 337–345.

[36] S. Komaba, T. Hasegawa, M. Dahbi, K. Kubota, Potassium intercalation into graphite to realize high-voltage/high-power potassium-ion batteries and potassium-ion capacitors, Electrochemistry Comm 60 (2015) 172–175.

[37] S. Oswald, M. Hantusch, M.V. Gorbunov, T. Schmeida, A. Thomas, D. Mikhailova, Electron spectroscopic investigations of alkaline-based battery-relevant reference materials, Surf. Interface Anal. 57 (2025) 439–444.